Molecular Plant
Research Article

CellPress
Partner Journal

The *miR166–SlHB15A* regulatory module controls ovule development and parthenocarpic fruit set under adverse temperatures in tomato

Christian Clepet[1], Ravi Sureshbhai Devani[1], Rachid Boumlik[1], Yanwei Hao[1,5], Halima Morin[1], Fabien Marcel[1], Marion Verdenaud[1], Brahim Mania[1], Gwilherm Brisou[1], Sylvie Citerne[4], Gregory Mouille[4], Jean-Christophe Lepeltier[2], Shai Koussevitzky[3], Adnane Boualem[1] and Abdelhafid Bendahmane[1,*]

[1]Institute of Plant Sciences Paris-Saclay, INRAE, CNRS, Université Paris-Saclay, Orsay 91405, France

[2]HM Clause, Mas Saint-Pierre, Quartier La Galine, Saint-Rémy de Provence 13210, France

[3]Hazera Seeds Ltd, Berurim M.P., Shikmim 7983700, Israel

[4]Institut Jean-Pierre Bourgin, INRAE, Versailles, France

[5]Present address: Key Laboratory of Horticultural Crop Biology and Germplasm Innovation in South China, College of Horticulture, South China Agricultural University, Guangzhou 510642, China

***Correspondence: Abdelhafid Bendahmane (abdelhafid.bendahmane@inrae.fr)**

https://doi.org/10.1016/j.molp.2021.05.005

ABSTRACT

Fruit set is inhibited by adverse temperatures, with consequences on yield. We isolated a tomato mutant producing fruits under non-permissive hot temperatures and identified the causal gene as *SlHB15A*, belonging to class III homeodomain leucine-zipper transcription factors. *SlHB15A* loss-of-function mutants display aberrant ovule development that mimics transcriptional changes occurring in fertilized ovules and leads to parthenocarpic fruit set under optimal and non-permissive temperatures, in field and greenhouse conditions. Under cold growing conditions, *SlHB15A* is subjected to conditional haploinsufficiency and recessive dosage sensitivity controlled by microRNA 166 (*miR166*). Knockdown of *SlHB15A* alleles by *miR166* leads to a continuum of aberrant ovules correlating with parthenocarpic fruit set. Consistent with this, plants harboring an *Slhb15a–miRNA166*-resistant allele developed normal ovules and were unable to set parthenocarpic fruit under cold conditions. DNA affinity purification sequencing and RNA-sequencing analyses revealed that SlHB15A is a bifunctional transcription factor expressed in the ovule integument. SlHB15A binds to the promoters of auxin-related genes to repress auxin signaling and to the promoters of ethylene-related genes to activate their expression. A survey of tomato genetic biodiversity identified *pat* and *pat-1*, two historical parthenocarpic mutants, as alleles of *SlHB15A*. Taken together, our findings demonstrate the role of *SlHB15A* as a sentinel to prevent fruit set in the absence of fertilization and provide a mean to enhance fruiting under extreme temperatures.

Key words: parthenocarpy, dosage sensitivity, HD-ZipIII, miRNA166, heat stress, cold stress

Clepet C., Devani R.S., Boumlik R., Hao Y., Morin H., Marcel F., Verdenaud M., Mania B., Brisou G., Citerne S., Mouille G., Lepeltier J.-C., Koussevitzky S., Boualem A., and Bendahmane A. (2021). The *miR166–SlHB15A* regulatory module controls ovule development and parthenocarpic fruit set under adverse temperatures in tomato. Mol. Plant. **14**, 1185–1198.

INTRODUCTION

In flowering plants, ovules are seed precursors made up of one or two sheathing integuments surrounding a nucellus in which meiosis, fertilization, and embryo development occur (Cooper, 1931). Ovule, seed, and fruit development are tightly coordinated. At anthesis the ovary stops cell divisions and enters a growth-arrest phase, or resumes cell division to develop into a fruit when pollinated (Joldersma and Liu, 2018). Fruit can develop independent of ovule fertilization in a process referred

Published by the Molecular Plant Shanghai Editorial Office in association with Cell Press, an imprint of Elsevier Inc., on behalf of CSPB and CEMPS, CAS.

to as parthenocarpy. This alternative pathway can be genetically controlled or artificially induced by phytohormones (Joldersma and Liu, 2018).

Reproductive organs are highly sensitive to environmental factors. In particular, heat stress affects anther development, style elongation, meiosis, pollen release, pollen germination, pollen-tube growth, pollen–pistil interaction, fertilization, endosperm formation, and embryo development, with consequences on fruit set (e.g., Abdul-Baki and Stommel, 1995; Sato et al., 2000; Erickson and Markhart, 2002; Firon et al., 2006; Zinn et al., 2010; Giorno et al., 2013). On average, global yields will fall by 3%–7.4% for each degree-Celsius increase (Zhao et al., 2017a). Cold stress also severely hampers the development of reproductive organs, causing severe necrosis, homeotic-floral transformations, and poor pollen germination (Zinn et al., 2010). Improving flower fertilization and fruit set under a wider range of temperatures can help achieve year-round cropping and, more importantly, maintain a sustainable agriculture in the scenario of a 2°C to 4°C increase, projected for 2100 (Zhao et al., 2017a).

In tomato (*Solanum lycopersicum*) the fruit set is strongly hindered at temperatures above 29°C (Peet et al., 1998) or lower than 12.8°C (Charles and Harris, 1972). Because of these limitations, tomato cultivation is restricted to certain geographic areas and time of the year (Joldersma and Liu, 2018). Tomato fruit set relies on a complex regulation involving positive and negative growth factors. Notably, pollination induces a burst of auxin and gibberellin (GA) biosynthesis and, as suggested by various studies, auxin promotes ovary growth at least partially by increasing GA synthesis (Serrani et al., 2008; Dorcey et al., 2009). More recently the gaseous hormone ethylene was proposed to connect auxin and GA, preventing GA perception and fruit set (Shinozaki et al., 2018). The ovule has a predominant role in this developmental program; the burst of auxin and GA is mainly produced by the young embryo or surrounding tissue (Dorcey et al., 2009; Pattison et al., 2015; Zhang et al., 2016), whereas in the absence of fertilization, ethylene is produced, promoting ovule senescence and flower drop (Carbonell-Bejerano et al., 2011). These facts were drawn in part from the knockdown of the *AUXIN RESPONSE FACTOR 7* (*ARF7*) (de Jong et al., 2009) or *DELLA* (Marti et al., 2007), or by inducing the expression of auxin (Rotino et al., 1997) or GA biosynthesis enzymes (Garcia-Hurtado et al., 2012). Together with hormones, gene-regulatory networks are recruited to control fruit set. These include transcription factors modulated post-transcriptionally by microRNAs (miRs; Jones-Rhoades et al., 2006). For instance, tomato lines overexpressing *miR167*, targeting *ARF6/8*, are unable to generate fruits (Liu et al., 2014). In contrast, tomato lines overexpressing *miR159*, targeting *GAMYB1/2*, display obligatory parthenocarpy (da Silva et al., 2017). Nevertheless, the mechanisms through which unfertilized ovules interfere with fruit development are still poorly characterized. We report a new regulatory module, in which *miR166* and *SlHB15A* control ovule development and fruit set, in tomato. *SlHB15A* loss-of-function mutants exhibit aberrant ovules and parthenocarpic fruits under adverse temperature conditions. *SlHB15A* is also dosage sensitive under cold conditions. We demonstrate that this process implicates the cold induction of *miR166*, knocking down *SlHB15A*, and consequently leading to fruit set. Transcriptome analysis as well as genome-wide identification of SlHB15A direct targets showed that SlHB15A acts as a bifunctional transcription factor, modulating auxin and ethylene signaling to interfere with fruit set in the absence of fertilization.

RESULTS

Tomato pf1 mutant produces fruits under non-permissive hot conditions

Although tomato can grow in a wide range of environments, the reproductive phase is highly sensitive to non-optimal low and high temperatures (Charles and Harris, 1972; Peet et al., 1998; Zinn et al., 2010). To identify fertilization-independent fruit set, we screened an ethyl methanesulfonate (EMS)-mutagenized population under non-permissive heat conditions. One mutant line, named hereafter *parthenocarpic fruit 1* (*pf1*), set seedless fruits and was further investigated in an insect-proof and temperature-controlled greenhouse. Following stamen ablation, flowers in the *pf1* line developed into seedless fruits, while flowers of the M82-parental line showed no fruit set (Figure 1A–1H). Extended phenotyping of *pf1* fruits revealed no obvious developmental phenotypes but the fruits were smaller and more abundant (Supplemental Figure 1). Some of the ripe fruits displayed malformations (Supplemental Figure 1H, 1K, and 1M) but these defects were not seen when *pf1* was introgressed in medium-fruited and cherry-sized round-tomato cultivars, likely due to interaction with fruit-shape genes (Rodriguez et al., 2011) (Figure 1E–1H and Supplemental Figure 1B). Synchronous fruit set and ripening are key traits in processing tomato breeding. Interestingly, *pf1* produced twice the amount of ripe fruits at harvest than the wild type (WT) (Supplemental Figure 1J, 1L, and 1M and supplemental methods), likely because fertilization is not required. Further phenotyping of vegetative and flowering traits is discussed in the supplemental methods and Supplemental Figure 2.

In addition to high temperatures, hot nights and small differences between night and day temperatures are well known to interfere with fruit set. We tested whether the *pf1* allele confers fruiting advantage at 32°C/24°C day/night, non-permissive conditions. In contrast to WT, *pf1* plants were able to set fruits (Figure 1I–1P).

PF1 encodes an HD-ZipIII transcription factor

Backcrossing and segregation analysis identified *pf1* as a single-locus-recessive mutation (Supplemental Figure 1A). To identify the causal mutation, we sequenced bulked-genomic DNA from parthenocarpic and non-parthenocarpic M2 plants and determined the Δ(SNP-index) (Figure 1Q and 1R and Supplemental Figure 3). Fine mapping further delimited *pf1* to a single gene, *SolyC03g120910*, harboring an EMS-induced G3872A transition. This one-base transition leads to a premature stop codon, W411*, suggesting that *pf1* is a null allele. Protein alignment and phylogenetic analysis revealed that *SolyC03g120910* encodes a class III homeodomain leucine-zipper (HD-ZipIII) protein, named hereafter *SlHB15A*, in reference to *AtHB15*, the closest homolog in *Arabidopsis thaliana* (Supplemental Figure 4A and 4B), and the nomenclature of HD-ZipIII proteins (Xu et al., 2019).

To confirm the role of *SlHB15A* in fruit set, we screened the gene for induced mutations, using the targeting induced local lesions in

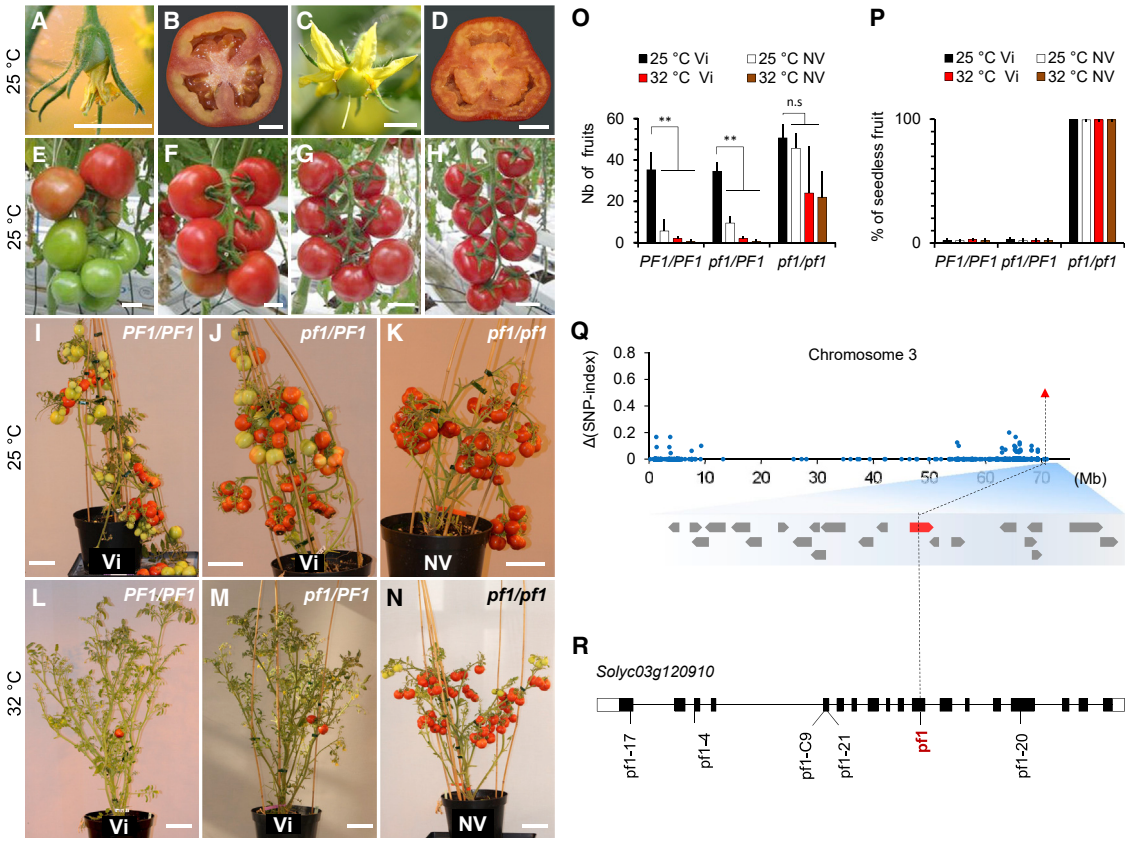

Figure 1. *pf1* confers obligate parthenocarpy under adverse heat conditions.

(A–N) Developing and mature fruits from WT fertilized flowers **(A and B)** and *pf1/pf1* unfertilized flowers **(C and D)**. Parthenocarpic fruit is seedless **(D)** and develops on top of the corolla **(C)**. Introgression of the *pf1* allele in fresh-market **(E and F)** and cherry **(G and H)** tomatoes leads to parthenocarpic fruit set **(F, H)**. **(E and G)** *PF1/PF1* WT pollinated fruits. **(A to H)** Plants grown at 25°C. Fruit set of pollinated (Vi) and unpollinated (NV) tomato genotypes grown at 25°C **(I–K)** or 32°C **(L–N)**. Leaves were removed to show the fruits.

(O) Number of developed fruits per plant. $^{**}P < 0.01$; n.s, no statistically significant difference.

(P) Percentage of seedless fruits at harvest for each genotype grown at 25°C or 32°C. Values are means ± SD derived from five plants. Two-tailed unpaired Student's *t*-test was used to determine the significance of the indicated comparisons.

(Q) Distribution of Δ(SNP-index) long chromosome 3, calculated with a 1-Mb sliding window. The highest genome-wide Δ(SNP-index) (red triangle) corresponds to a G-to-A nonsense mutation in the gene *Solyc03g120910*. Arrows show the annotated genes on both chromosome strand.

(R) Structure of *PF1/SlHB15A* gene and induced alleles leading to obligate parthenocarpy. UTRs and coding sequence are indicated as hollow and filled boxes, respectively. Scale bars represent 1 cm in **(A–D)**; 2 cm in **(E–H)**; 10 cm in **(I–N)**.

genomes (TILLING) and clustered regularly interspaced short palindromic repeats (CRISPR)-Cas9 approaches. Of 62 alleles we isolated (Supplemental Table 1), 26 were predicted to induce changes in the amino acid sequence and were backcrossed to WT. Segregant plants were then phenotyped for fruit set. As expected, plants homozygous for nonsense, splicing, deletion, or deleterious-missense mutations were parthenocarpic (Supplemental Figure 5), validating the role of *SlHB15A* in inhibition of fruit set in the absence of fertilization.

To assess the level of polymorphism at *SlHB15A*, we examined the sequence diversity of the coding region in a panel of 401 accessions that included nine lines previously described as parthenocarpic or seedless. We identified five gene variants, leading to four missenses and one codon deletion (Supplemental Table 2). Three missense mutations, C561G, L712S, and P805L, were predicted not to impact the function of the protein, and plants harboring these mutations did not set fruits in the absence of pollination. Interestingly, two other mutations, a G583R missense and an A567 deletion, were revealed respectively in two accessions, *pat* (Soressi and Salamini, 1975) and *pat-1* (Pecaut and Philouze, 1978), previously described as parthenocarpic (Supplemental Table 3). Next, we crossed *pat* and *pat-1* to *pf1* to test if they were allelic. For each cross at least 10 F1 plants and 10 manually castrated flowers per plant were phenotyped for parthenocarpic fruit set. We found all F1-hybrid plants were parthenocarpic, confirming that *pat*, *pat-1*, and *pf1* are all alleles of *SlHB15A*.

SlHB15A-hypomorphic alleles exhibit parthenocarpy under cold growing conditions

Although low temperatures are a prerequisite for floral induction in many species (Xu and Chong, 2018), cold stress is a devastating factor for fruit set (Charles and Harris, 1972). To test whether *SlHB15A* alleles can confer fruiting advantage under cold growing conditions, plants were grown at 15°C day/12°C night (cold stress) and phenotyped for fruit set. These

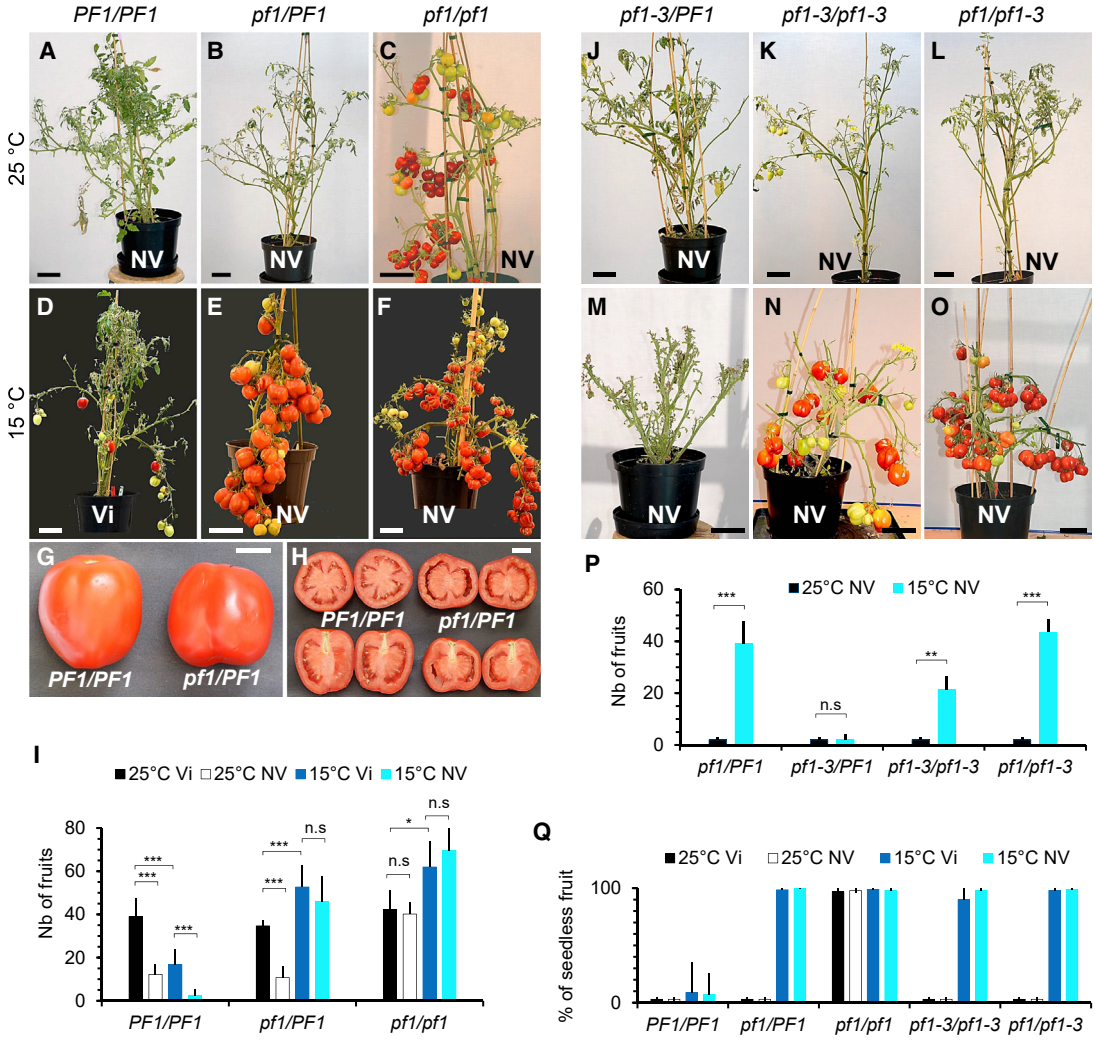

Figure 2. *pf1* alleles confer conditional parthenocarpy under cold conditions.

Fruit set of tomato genotypes grown at 25°C **(A–C and J–L)** or 15°C **(D–F, M–O)**. In *pf1/pf1* plants, parthenocarpic fruits develop under any conditions **(C and F).** Conditional parthenocarpy occurs in *pf1* heterozygous plants only at 15°C **(E)**, yielding fruits similar in size (**G and H**, right) to pollinated fruits (G and H, left). *pf1-3* hypomorphic allele, not parthenocarpic under optimal temperature **(J–L)**, expresses conditional parthenocarpy at 15°C **(N and O).** Number of ripe fruits per plant **(I and P)** and percentage of seedless fruits **(Q)** at harvest are shown for each genotype and stress condition. Vi, pollinated; NV, unpollinated. Values are means ± SD derived from at least six plants. Two-tailed Student's *t*-test was used to determine the significance of the indicated comparisons. $^{*}P < 0.05$, $^{**}P < 0.01$, $^{***}P < 0.001$; n.s, no statistically significant difference. Plants were defoliated to show the fruits. Scale bars represent 10 cm in **(A–O)**; 2 cm in **(G and H)**.

unfavorable conditions decreased the fruit set by ~60% in WT pollinated control plants, while *SlHB15A* loss-of-function mutants were not affected (Figure 2A–2H). We even observed an increase in fruit set of up to 70% in *pf1* plants, compared with control plants (Figure 2I). Unexpectedly, plants harboring loss-of-function mutations at a heterozygous state were parthenocarpic, suggesting that *SlHB15A* is haploinsufficient to inhibit fruit set under cold stress (Figure 2E and Supplemental Figure 6A). To test whether this cold-induced parthenocarpy also occurs under field-growing conditions, we cultivated four *SlHB15A* mutants, *pf1*, *pf1-4*, *pf1-17*, and *pf1-20*, showing recessive parthenocarpy under optimal temperature, in winter over two seasons (Supplemental Figure 6C–6E). As for plants grown under greenhouse conditions, all four heterozygous mutants were parthenocarpic during winter cultivation. Unlike *pf1* homozygotes, parthenocarpic fruits of *pf1* heterozygote plants were similar in size to fruits of WT plants grown under optimal conditions, and did not show any malformation (Figure 2G and 2H and Supplemental Figure 6B).

The sensitivity of *SlHB15A* to gene dosage suggests that hypomorphic alleles, such as N92Y (*pf1-3*), may still lead to parthenocarpy under cold growing conditions. The N92Y mutation is located in the leucine-zipper domain, predicted to be required for SlHB15A dimerization; still, plants homozygous for the N92Y mutation are not parthenocarpic under optimal or hot conditions (Supplemental Figure 5). Under cold growing conditions, the N92Y mutant was parthenocarpic only at the homozygous state, and *pf1/pf1-3* compound heterozygotes exhibited strong induced parthenocarpy (Figure 2J–2Q), in line with the *pf1* heterozygous mutant phenotype. *pf1/pf1-3* hybrids were never scored as parthenocarpic under optimal or hot conditions

(Supplemental Table 4). Consistent with this, two other hypomorphic alleles, *pf1-2* and *pf1-16*, non-parthenocarpic under hot and control conditions (Supplementary Table 4), were found to be parthenocarpic in the winter field test (Supplemental Figure 6F). We refer to this cold-induced parthenocarpy as conditional parthenocarpy (supplemental methods).

miR166 is a cold-inducible switch of parthenocarpy in tomato

Next, we investigated whether this gene-dosage effect was dependent on *SlHB15A* mRNA accumulation under cold stress. Thus, we analyzed the *SlHB15A* expression pattern in developing flowers, from stage 1 to 4 days after anthesis (DAA), as well as in leaf and shoot apex. We found uniform and ubiquitous accumulation, using quantitative polymerase chain reaction (qPCR) (Figure 3A and Supplemental Figure 7A). However, spatial expression analysis using *in situ* hybridization pinpointed localized accumulations. *SlHB15A* mRNA was detected in shoot–apical meristem, sympodial meristem, and vascular elements. The strongest expression was detected in transition meristem, inflorescence meristem, and flower–meristem dome (Figure 3K–3N and Supplemental Figure 7B–7D). Expression was also observed in ovule primordia and in the outer cell layer of the ovule integument (Figure 3O and 3P and Supplemental Figure 7E).

As mRNA accumulation of HD-ZipIII transcription factors is known to be controlled by *miR166s* (Kim et al., 2005), we analyzed tomato reproductive organ degradomes (Lopez-Gomollon et al., 2012) and revealed a *SlHB15A* cleavage site matching *miR166* pairing (Figure 3B). Because *miR166* was reported to control development (Hashimoto et al., 2018) and modulate plant responses to abiotic stresses, including low temperature (Omidvar et al., 2015), we investigated whether *miR166* controls conditional parthenocarpy under cold growing conditions. Using *in situ* hybridization, we revealed overlapping expression of *miR166* and *SlHB15A* in a range of tissues, including sympodial, inflorescence, and flower meristems, as well as developing flowers (Figure 3C, 3D, 3K, and 3L and Supplemental Figure 7). qPCR analysis revealed cold-induced expression of *miR166* (Figure 3Q) but failed to show reproducibly reduced accumulation of *SlHB15A* mRNA under cold conditions (supplemental methods and Supplemental Figure 7M). We therefore used genetics to demonstrate that *miR166* is the cold-inducible switch of *SlHB15A* dosage sensitivity. In order to not alter the expression of *SlHB15A*, we used TILLING to screen for *SlHB15A miR166*-resistant alleles. We isolated a line, *pf1-6*, harboring a C2672T substitution that disrupts the complementarity with *miR166* (Figure 3B and Supplemental Figures 5 and 8A–8J). Even though C2672T is a non-synonymous mutation, it leads to a conserved mutation that does not confer parthenocarpy at any condition (Figure 3G and 3H). In line with *pf1-6* is an *miR166*-resistant allele, the pf1-6 homzygous mutant displayed no mRNA reduced accumulation, concurrent with the *miR166* induction, and an *miR166*-resistant mutation identical to *pf1-6* was described in another HD-ZipIII transcription factor, *Oryza sativa* lateral floret 1 (*OsLF1*) (Zhang et al., 2017) (Figure 3Q and Supplemental Figure 8B and supplemental methods). By crossing *pf1-6*/*pf1-6* and *pf1*/*pf1* homozygotes, we generated compound heterozygote *pf1*/*pf1-6* plants that we phenotyped for parthenocarpy under cold conditions (Figure 3E–3J and Supplemental Figure 8K). None of the hybrid plants set fruits in the absence of fertilization (Figure 3S), validating genetically that *miR166* is the cold-inducible switch leading to parthenocarpy. To further demonstrate the reduced accumulation of *SlHB15A* mRNA under cold conditions, we took advantage of *PF1*/*pf1-6* heterozygote plants. We predicted that even small and transient induction of *miR166* under cold conditions should lead to measurable differences in the relative accumulation of mRNAs from the two alleles. The difference should also be exaggerated under cold stress. Thus, we conducted a comparative transcriptomic analysis of flowers of *PF1*/*pf1-6* heterozygote plants grown under cold stress or control conditions (supplemental methods). We found *pf1-6* mRNA accumulating on average 1.5-fold more than *SlHB15A* mRNA, under cold stress, confirming that *pf1-6* is indeed *miR166* resistant. These data also demonstrate that the cold stress leads to the reduced accumulation of *SlHB15A* mRNA (Figure 3R). Collectively, these data demonstrate that *miR166* is likely to be the cold-inducible switch leading to *SlHB15A* dosage sensitivity and parthenocarpy.

A gradient of aberrant ovules correlates with parthenocarpy

As *SlHB15A* is highly expressed in ovule integument, we examined the ovules of *SlHB15A* mutants. Prior to integument initiation at stage 11, no visible ovule alteration was observed (Supplemental Figure 9A and 9B). In contrast, at stages 18 and 20, most *pf1* ovules are orthotropous and the integument is aborted, remaining at the base of the nucellus (Figure 4A–4C, Supplemental Figure 9G, and supplemental methods). In line with the lack of integument in aberrant ovules, the integument marker gene, *INNER NO OUTER* (*INO*) (Skinner et al., 2016), was not expressed in *pf1* dissected ovules (Supplemental Figure 9U). Ovule defects have been correlated with parthenocarpy in tomato; however, whether defective ovules are the cause of the parthenocarpy remained an open question (da Silva et al., 2017; Hao et al., 2017; Wang et al., 2009). We exploited the conditional *SlHB15A* parthenocarpy to assess the extent to which aberrant ovules correlate with parthenocarpy. Plants harboring different *SlHB15A*-allelic combinations were cultivated under optimal and cold growing conditions and phenotyped for aberrant ovule development. We found less than 1% of aborted ovules in WT plants. In contrast, *pf1*/*pf1* homozygous plants exhibited 91% aberrant ovules at 25°C and 95% under cold stress (Figure 4F, 4I, and 4J and Supplemental Figure 9). *pf1*/*PF1* heterozygotes behaved like WT at 25°C, but under cold conditions more than 50% of the ovules were aberrant (Figure 4E, 4H, and 4J and Supplemental Figure 9). Plants homozygous for the *pf1-3* hypomorphic allele showed no ovule phenotype at 25°C and a small but significant number of aberrant ovules under cold stress (20%; Figure 4J and Supplemental Figure 9N and 9Q). *pf1*/*pf1-3* ovaries displayed only a few aberrant ovules at 25°C (2.9%), whereas under cold, they harbored almost as many as the *pf1*/*pf1* genotype (83%; Figure 4J and Supplemental Figure 9O and 9R). Since *pf1*/*pf1-6* plants harbored normal ovules under both conditions, we concluded that the *pf1-6 miR166*-resistant allele protects against parthenocarpy as well as aberrant ovule development under cold conditions (Figure 4J and Supplemental Figure 9L

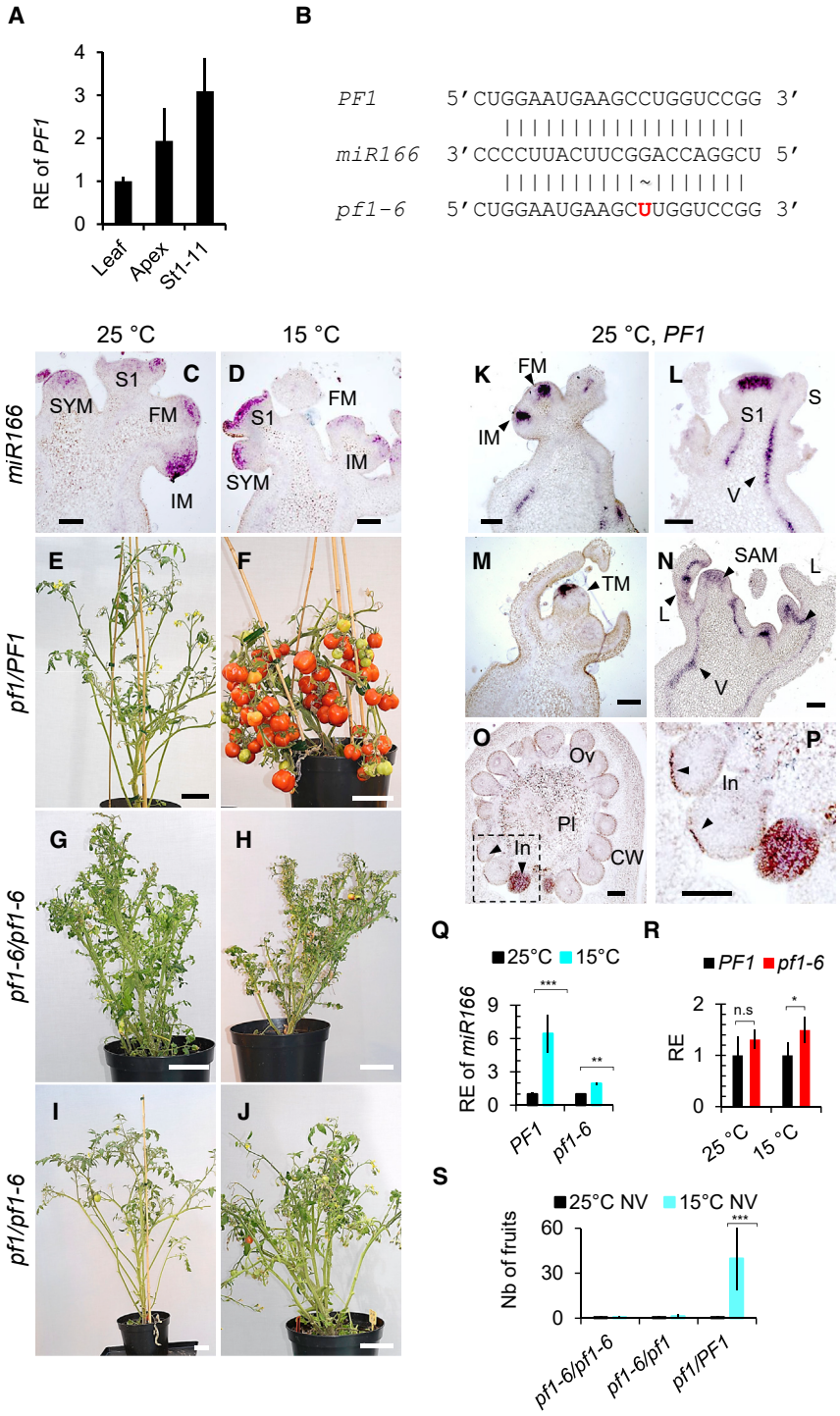

Figure 3. Cold-induced *miR166* controls *SlHB15A*-mediated parthenocarpy.

(A) Expression analysis of *PF1* in leaf, shoot apex, and stage 1–11 flowers (St1–11). Values are means ± SD derived from three plants. RE, relative expression.

(B) *miR166* base pairing with *PF1* and *miR166*-resistant *pf1-6* transcripts.

(C, D, and K–P) *In situ* hybridization of *miR166* **(C and D)** and *PF1* **(K–P)** in shoot apex and flower. **(O)** Stage 16 ovary. **(P)** Ovule magnification. IM, FM, TM, SYM, and SAM indicate inflorescence, flower, transition, sympodial, and shoot apical meristems, respectively. S1, stage 1 flower–meristem dome; V, vascular element; In, integument outer-cell layer; CW, carpel wall; Ov, ovule; Pl, placenta; L, leaf; S, sepal. Bars, 100 μm. Arrowheads highlight PF1 expression.

(E–J) Fruit set of unpollinated (NV) tomato genotypes at 25°C **(E, G, and I)** or 15°C **(F, H, and J)**. Leaves were removed to show the fruits. Bars, 10 cm.

(Q) qPCR analysis of *miR166* transcripts in 3-week-old apices of *PF1/PF1* and *pf1-6/pf1-6* plants grown at 15°C or 25°C. Values are means ± SD derived from three plants.

(R) Relative abundance assessed by RNA sequencing (RNA-seq) of WT *PF1* versus *miR166*-resistant *pf1-6* transcripts in *PF1/pf1-6* heterozygotes grown at 25°C or 15°C. Values are means ± SD of *PF1* and *pf1-6* reads spanning the *pf1-6* mutation locus derived from three RNA-seq experiments. RE, relative expression.

(S) Number of seedless fruits per plant. Values are means ± SD derived from nine plants. Two-tailed Student's *t*-test was used to determine the significance of the indicated comparisons. $^{*}P < 0.05$, $^{**}P < 0.01$, $^{***}P < 0.001$; n.s, no statistically significant difference.

and 9P). Altogether, these data point to *miR166* inactivation of *SlHB15A* to a threshold leading to aberrant ovule development and consequently to parthenocarpy.

Aberrant ovules mimic pollinated ovules

SlARF7 is a key marker gene of flower fertilization, expressed in ovules at the anthesis stage and downregulated after pollination (de Jong et al., 2009). To analyze to what extent aberrant ovules behave like fertilized ovules, we measured the expression of *SlARF7* in *pf1* ovules and found downregulation like in WT fertilized ovules (Supplemental Figure 9S and 9V). To extend this analysis, we compared the transcriptome of *pf1* ovules to unfertilized WT ovules, which revealed 3391 differentially expressed genes (DEGs; 1879 upregulated and 1512 downregulated) (Supplemental Figure 10 and Supplemental Table 6). Then, the obtained DEGs were compared with the 851, 1979, and 3325 DEGs obtained in the comparison of fertilized versus unfertilized WT ovules, collected at 1, 2, or 5 days post-pollination (DPP) (Zhang et al., 2016), respectively. A strong transcriptome overlap increasing from 1 to 5 DPP, with a *P* value close to 0 at 5 DPP was obtained (Figure 5A and Supplemental Figure 10). Gene ontology (GO) analysis on shared DEGs revealed enrichment for GO terms related to signaling and response to auxin in the upregulated genes, and response to ethylene in the downregulated genes, in line with their role in fruit-set control (Figure 5B) (Joldersma and Liu,

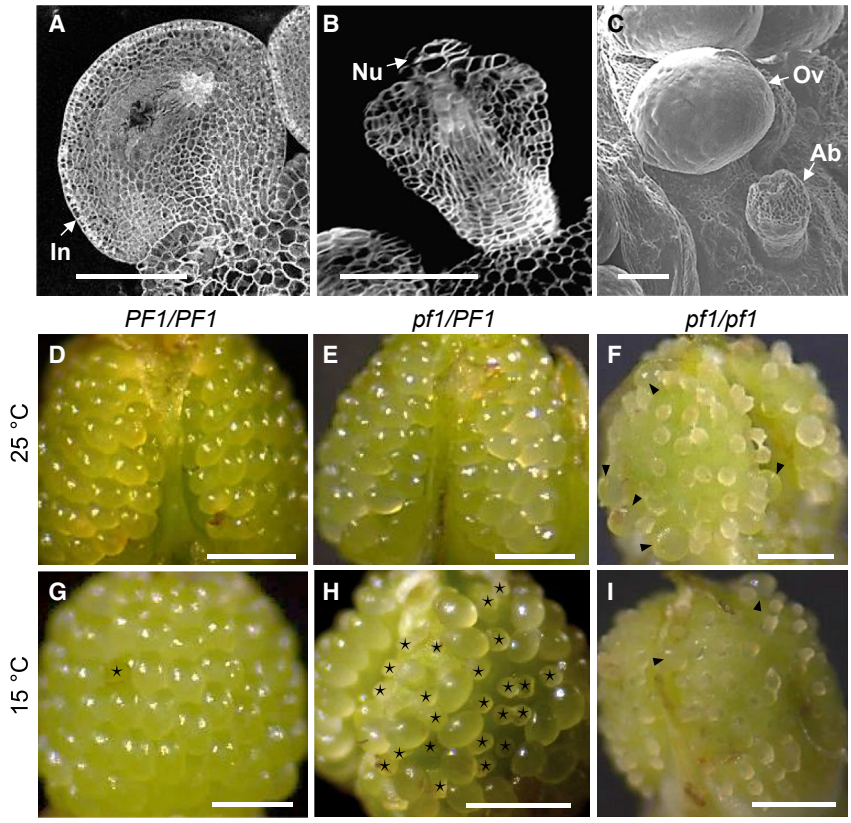

Figure 4. A gradient of aberrant ovules correlates with parthenocarpy in *pf1* plants.

(A and B) Confocal images of stage 18 WT anatropous (**A**) and *pf1*-aberrant ovule showing no integument (In) and uncovered nucellus (Nu) **(B)**.

(**C**) Scanning electron micrograph of anthesis normal-looking (Ov) and aberrant (Ab) ovules in *pf1*/*pf1*.

(D–I) Light micrographs of dissected ovaries developed under optimal (25°C, **D–F**) or cold (15°C, **G–I**) conditions. Asterisks highlight aberrant ovules in **(H)**, arrowheads normal ovules in **(F and I)**.

(J) Parthenocarpy and ovule phenotypes of various *pf1*-allele combinations under optimal and cold conditions. Mean percentages ± SD were averaged from at least three series of two ovaries. Different letters represent statistically significant differences within each temperature condition, according to one-way ANOVA with Tukey's *post hoc* test ($P < 0.01$). Scale bars, 100 μm **(A–C)** and 500 μm **(D–I)**.

J

	25 °C day/ 18 °C night		15 °C day/ 12 °C night	
Genotype	Parthenocarpy	Aberrant Ovule	Parthenocarpy	Aberrant Ovule
PF1/PF1	No	0.4 ±0.7% a	No	0.3 ±0.4% a
pf1/PF1	No	0.1 ±0.3% a	Yes	51.1 ±17.7% b
pf1/pf1	Yes	91.3 ±0.9% b	Yes	95.4 ±0.9% c
pf1-3/PF1	No	0.3 ±0.4% a	No	0.4 ±0.7% a
pf1-3/pf1-3	No	0.3 ±0.4% a	Yes	20.4 ±5.1% d
pf1/pf1-3	No	2.9 ±1.3% c	Yes	83.2 ±8.4% e
pf1/pf1-6	No	0.3 ±0.4% a	No	0.3 ±0.4% a

2018). Additional enrichment was observed for cell cycle, microtubule-based process, and polysaccharide metabolic process in the upregulated genes. In summary, the strong transcriptome overlap shows that *pf1* aberrant ovules mimic fertilized ovules, and this likely implicates *SlHB15A* as a key hormone regulator, repressing auxin and activating ethylene biosynthesis and signaling in ovules.

To test whether *SlHB15A* directly controls the auxin and the ethylene pathways in unfertilized ovules, we mapped genome-wide SlHB15A DNA binding, using DNA affinity purification sequencing (DAP-seq) (Supplemental Table 7). A total of 14 692 highly reliable SlHB15A-binding sites, mostly in the 5′ vicinity of the transcription start site of 4254 unique genes, were identified (Figure 5C and Supplemental Figure 11). A consensus motif ($P = 1 \times 10^{-6266}$) computed from >80% of these sequences encompasses the binding site previously characterized by DAP-seq for *Arabidopsis* AtHB15 (O'Malley et al., 2016) (Figure 5D) and, *in planta*, by chromatin immunoprecipitation sequencing for the *Arabidopsis* SlHB15A homolog, REVOLUTA (Brandt et al., 2012). We next integrated these data with our transcriptomic analysis and identified 270 and 202 genes that were both bound by SlHB15A and up- or downregulated in *pf1* ovules, respectively (Figure 5E). GO analysis further revealed strong enrichment of terms related to auxin biosynthesis, transport, and signaling in the upregulated genes and ethylene biosynthesis and signaling in the downregulated genes, revealing the role of *SlHB15A* in repression of auxin and induction of ethylene pathways in unfertilized ovules (Supplemental Figure 11C). In particular, auxin biosynthesis genes, such as *TOMATO FLOOZY 2* (*ToFZY2*) and *ToFZY3*, were found to be bound by SlHB15A and upregulated in WT fertilized and in *pf1* ovules (Figure 5F and Supplemental Figure 11D). Likewise, the auxin response factor *SlARF7* was bound by SlHB15A and downregulated in WT fertilized and in *pf1* ovules (Figure 5F and Supplemental Figure 9S and 9V). Conversely, the ethylene biosynthesis and signaling genes, such as *1-AMINOCYCLOPROPANE-1-CARBOXYLIC ACID OXIDASE 4 (ACO4)*, *ETHYLENE INSENSITIVE 3-LIKE 2 (EIL2)*, and *ETHYLENE RESPONSE FACTOR 1* (*SlERF.1*), were bound by SlHB15A and downregulated in fertilized and *pf1* ovules (Figure 5F and Supplemental Figure 11E). To validate the binding of SlHB15A to the identified auxin and ethylene genes, we used electrophoretic mobility-shift assay (EMSA). SlHB15A protein was produced in *Escherichia coli*, in fusion to *glutathione S-transferase* (GST), and incubated with biotin-labeled *cis*-regulatory elements identified in DAP-seq. We tested the binding to two auxin biosynthesis genes, *ToFZY2* and *ToFZY3*; the auxin transporter, *PIN FORMED 4* (*SlPIN4*); and the auxin response factor *SlARF7*. For ethylene, we tested three ethylene response factors, *SlERF.F1*, *SlERF.B13*, and *SlERF.H12*. Strong band shifts were obtained for all the probes and only when the biotin-labeled probes were incubated

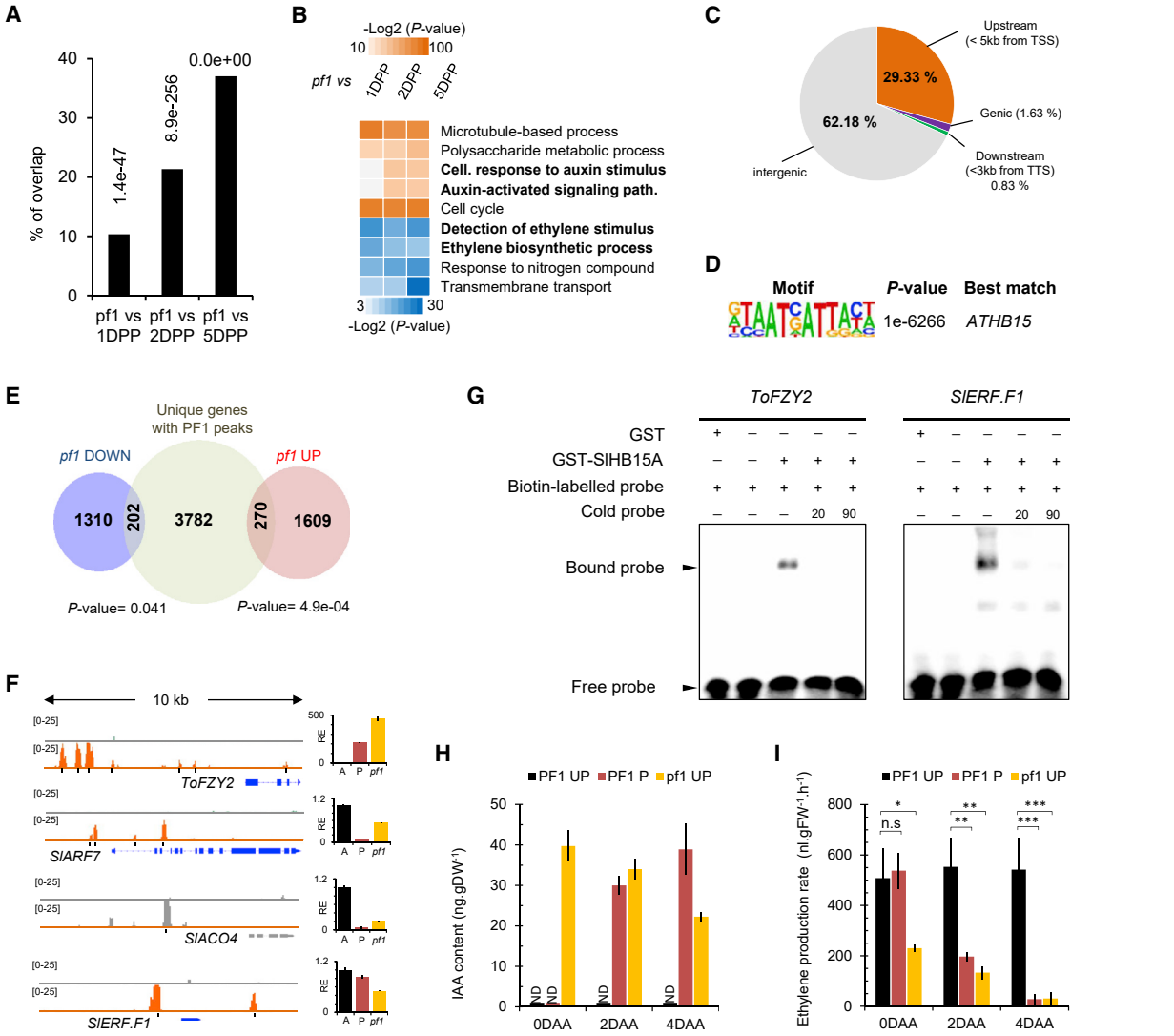

Figure 5. *pf1* aberrant ovules mimic fertilized ovules.

(A) Shared DEGs between *pf1* aberrant versus WT unfertilized ovules and WT unfertilized versus pollinated ovules at 1, 2, and 5 days post-pollination (DPP).

(B) GO analysis of the upregulated (orange) and downregulated (blue) genes.

(C) Analysis of PF1-enriched regions in the DAP-seq assay. Pie chart showing the percentage distribution of PF1-binding peaks in each category.

(D) PF1 DNA-binding motif.

(E) Overlap between the up- and the downregulated genes in *pf1* aberrant ovules and PF1-bound genes. Hypergeometric test *P* values are indicated.

(F) Genome browser view of the distribution of the DAP-seq reads (gray, HALO control; orange, PF1) of auxin and ethylene genes and their corresponding relative expression (RE) in aberrant ovules (*pf1*) and WT ovules at anthesis (A) or at 5 DPP (P).

(G) EMSAs showing that SlHB15A binds to the *ToFZY2* and *SlERF.F1 cis*-regulatory elements. Competition for binding was performed using 20 pmol and 90 pmol of unlabeled probes. GST was used as negative control.

(H and I) Indole-3-acetic acid (IAA) content **(H)** and ethylene production **(I)** in WT *PF1* fertilized (P) and unfertilized (UP) ovaries and *pf1* unfertilized (UP) ovaries at 0, 2, and 4 days after anthesis (DAA). ND, not detected. Two-tailed Student's *t*-test was used to determine the significance of the indicated comparisons. $^{*}P < 0.05$, $^{**}P < 0.01$, $^{***}P < 0.001$; n.s, no statistically significant difference. DW, dry weight; FW, fresh weight.

with SlHB15A protein, and not with GST (Figure 5G and Supplemental Figure 11F). The band shift disappeared in a competition experiment with increased concentration of unlabeled probes (Figure 5G and Supplemental Figure 11F). To test whether the control of the expression of auxin and ethylene genes has consequences on hormone production, we measured auxin and ethylene in ovaries of *pf1* and control plants at 0, 2, and 4 DAA. Consistent with ethylene negatively correlating with the progression of early fruit development, we found ethylene synthesized by pollinated *PF1* ovaries decreasing from 2 DAA onward (Figure 5I). Likewise, and consistent with early fruit development, we measured a low level of ethylene from the anthesis stage onward in *pf1* ovaries (Figure 5I). Consistent with auxin correlating with the progression of early fruit development, we found auxin synthesized by pollinated *PF1* ovaries increasing from 2 DAA, and *pf1* ovaries accumulating a high concentration of auxin from anthesis onward (Figure 5H).

DISCUSSION

We isolated a mutant producing parthenocarpic fruits at non-permissive temperatures and identified the causal mutation in an HD-ZipIII transcription factor, *SlHB15A*. Based on a large spectrum of alleles, we could show that *SlHB15A* confers both obligate and conditional parthenocarpy under controlled and field conditions (supplemental methods). At homozygous state, *SlHB15A* loss-of-function alleles, such as *pf1* or *pf1-4*, were found to lead to obligate parthenocarpy under optimal and non-permissive temperatures. At heterozygous state, the same alleles were found to lead to parthenocarpy only under cold growing conditions. We also found that weak alleles, such as *pf1-3* and *pf1-16*, lead to parthenocarpy only at the homozygous state and under non-permissive cold conditions. Later, we demonstrated, using an *Slhb15a-miR166* resistant line, that this conditional parthenocarpy is controlled by the cold induction of *miR166*, knocking down the *SlHB15A* transcript. *pf1-3* harbors a missense mutation in a highly conserved leucine-zipper residue, which could partially affect the function of the protein. In line with this, we could evidence that under optimal temperature, this hypomorphic allele confers a weak ovule phenotype in the context of the strong *pf1* allele (Figure 4 and Supplemental Figures 9 and 12). We explain these phenotypes by conditional gene-dosage effects. Whereas the haploinsufficiency of the strong alleles (*pf1*, *pf1-4, pf1-17*, *pf1-20*) is likely due only to the limiting amount of the transcript translated into WT protein, the dosage sensitivity of *pf1-3*, *pf1-16*, and *pf1-2* should be accounted for by both the altered protein function and the amount of transcript (Supplemental Figures 6 and 12).

Developmental processes are often controlled by tightly regulated dosage-sensitive genes (Johnson et al., 2019). Likewise, several genes involved in the development of the seed integument have already been associated with gene-dosage effects (Pillitteri et al., 2007; Wang et al., 2008; Zhao et al., 2017b). Conditional haploinsufficiency was also shown in yeast, in response to growth medium composition (Deutschbauer et al., 2005). Yet, to our knowledge the *miR166–SlHB15A* genetic system is the first report of conditional haploinsufficiency and recessive dosage sensitivity controlled by a microRNA.

SlHB15A loss-of-function mutants display aberrant ovules with aborted integument remaining at the base of the nucellus. In *Arabidopsis*, the development of the integument is also controlled by HD-ZipIII transcription factors, evidenced in the triple mutant *corona* (*cna*), *phabulosa* (*phb*), and *phavoluta* (*phv*) (Kelley et al., 2009). Systematic phenotyping of *SlHB15A* mutant plants under optimal or adverse temperature conditions revealed a gradient of 2%–95% defective ovules per ovary. Ovule defects were previously reported in other parthenocarpic mutants of tomato, such as the *INDOLE-3-ACETIC ACID 9* (*IAA9*) silencing line in which growth of the integument is affected (Wang et al., 2009); the *miR159–GAMYB1/2* transgenic system, which displays abnormal growth of the embryo sac (da Silva et al., 2017); or the *SPOROCYTELESS/NOZZLE* (*SPL/NZZ)* deletion mutant, which develops incomplete ovules lacking integument and a megaspore mother cell (Hao et al., 2017). In our case, by exploiting the cold-inducible parthenocarpy, we could demonstrate that defective ovules fully correlate with parthenocarpy. This is intriguing, pointing toward the role of *SlHB15A* and the integument in inhibiting the initiation of fruit set until fertilization. This also opens the question of how fertilization relieves the carpel from *SlHB15A*-mediated inhibition.

We found by transcriptome profiling that *pf1* aberrant ovules behave similar to WT pollinated ovules. Notably they share different members of gene families associated with the biosynthesis or signaling of auxin and ethylene hormones (Zhang et al., 2016; Joldersma and Liu, 2018). *cis*-regulatory elements and expression analyses further revealed that SlHB15A is a bifunctional transcription factor. We show that SlHB15A binds to a DNA motif, matching the consensus binding site previously described for AtHB15 (O'Malley et al., 2016) and another HD-ZIPIII transcription factor (Brandt et al., 2012). We found several auxin genes to be targeted by SlHB15A and differentially expressed; notably, two YUCCA-like flavin monooxygenases, *ToFZY2* and *ToFZY3*, are upregulated in fertilized flowers and in *pf1* loss-of-function mutants, consistent with auxin-biosynthesis transgenes leading to parthenocarpy (Rotino et al., 1997). We also found *SlARF7* targeted and downregulated in *pf1* ovules, also in line with the knockdown of *SlARF7* leading to parthenocarpy (de Jong et al., 2009). In accordance with SlHB15A repressing auxin biosynthesis genes, we found the levels of auxin in *pf1* ovaries, at anthesis stage, to be similar to the level of auxin in WT ovaries 2 DPP. In addition to auxin, we found *pf1* ovaries releasing low amounts of ethylene, and ethylene response factors, especially *SlERF.F1*, *SlERF.B13*, and *SlERF.H12*, targeted by SlHB15A and downregulated in *pf1* ovules, also consistent with ethylene acting as a negative fruit-set regulator (Shinozaki et al., 2018).

In *Arabidopsis*, the lack of integument in the *ats-1* mutant was associated with overaccumulation of GA (Gomez et al., 2016). To test whether the lack of integument in *SlHB15A* loss-of-function mutants is due to a GA accumulation, we analyzed the expression of *GA20 oxidase1* (*SlGA20ox1*), and the integument marker gene, *INO*. *SlGA20ox1*, is a key GA-biosynthesis gene induced following flower fertilization (Serrani et al., 2007; Okabe et al., 2019). Interestingly, we found an approximately two-fold increased expression of *GA20ox1* in *pf1* flowers from stage 11 onward (Supplemental Figure 13A), when integument initiation normally takes place (see "*INO* expression," Supplemental Figure 13B). We also found the expression of *SlGA20ox1* upregulated in *pf1* aberrant ovules and in dissected ovules plus placenta (Supplemental Figure 9T and 9V).

During the submission of this work, Shinozaki and colleagues reported on the role of a tomato *DELLA* homolog called *PROCERA* and its loss-of-function mutant, *procera* (*pro*), in parthenocarpic fruit set (Shinozaki et al., 2020). Interestingly *SlHB15A* was found to be downregulated in the parthenocarpic *pro* mutant. As the role of GA in fruit set is downstream of the role of auxin, it is still not clear how the developing fruit in the *pro* mutant interferes with the expression of *SlHB15A*. One possibility is that GA accumulation in the *pro* mutant interferes with the ovule/integument development where *SlHB15A* is expressed. In line with this, the ovule number was found to be reduced in both *pro* mutants and *GA20ox1*-overexpressing lines (Gomez et al., 2018 and Garcia-Hurtado et al., 2012). On the other hand, in the DAP-seq analysis, we did not find any direct

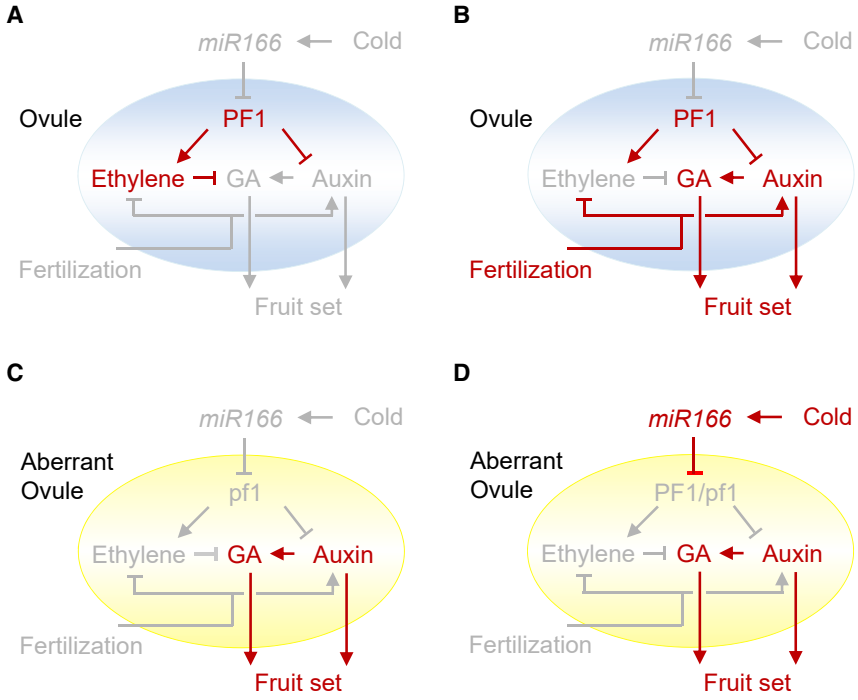

Figure 6. working model explaining how the *miR166–SlHB15* regulatory module controls ovule development and fruit set.

(A) In the absence of fertilization, PF1 inhibits auxin and activates ethylene signaling, maintaining the ovary in a growth-arrest phase until pollination takes place.

(B) Ovule fertilization relieves the inhibition; accumulation of auxin and inhibition of ethylene signaling lead to fruit set.

(C) *pf1* loss-of-function alleles induce aberrant ovules that mimic WT pollinated ovules.

(D) In *Pf1/pf1* heterozygote plants, under cold conditions, the overexpression of *miR166* knocks down *PF1* mRNA to threshold, leading to aberrant ovules and fruit set.

binding of SlHB15A to key GA biosynthetic or signaling genes, yet we found upregulation of the expression of *GA20ox1*. These data also suggest that GA biosynthesis or its signaling cascade, in the *pf1* mutant, is the consequence of auxin accumulation and/or ethylene repression (Hu et al., 2018; Serrani et al., 2008; Shinozaki et al., 2018).

In summary, our work identified *SlHB15A* as a sentinel against fruit set. In the absence of fertilization, *SlHB15A* inhibits auxin biosynthesis and activates biosynthesis of ethylene, maintaining the ovary in a growth-arrest phase. Inactivation of *SlHB15A* or pollination reverses the process, leading to auxin accumulation and repression of the ethylene response (Figure 6). As the *pf1* mutant accumulates auxin, at the anthesis stage, it is likely that fertilization interferes with the function of *SlHB15A*. It will be of interest to investigate the molecular mechanisms leading to this interference, for example, via identification of a repressor of *SlHB15A* function. Our investigation also led to the discovery of the *miR166–SlHB15A* regulatory module as a new tool to engineer facultative and obligate parthenocarpy in tomato (supplemental methods). This could be carried out through the expression of *miR166* under cold- or heat-inducible promoters. A survey of tomato germplasms identified *pat* and *pat-1*, two historical mutants, as alleles of *SlHB15A*. Finally, in addition to the large spectrum of alleles generated in this work, the knowledge generated could also be used as the base to develop plant prototypes producing fruit under adverse conditions.

METHODS

Plant materials and growth conditions

S. lycopersicum historical parthenocarpic or seedless mutants were provided by different germplasm distribution centers (see supplemental methods). The *pf1* mutant was isolated by screening a population of 1000 EMS-mutagenized plants derived from *S. lycopersicum* cv. M82.

Ten thousand M2 plants were cultivated to fruit maturity in open field. Blooming and fruit set occurred in June, under an average temperature of ~27°C (max 32°C/min 22°C), affecting significantly the fruiting in M82; harvest and seed counting were performed in August. For experiments within a controlled environment, plants were cultivated in pots filled with a mix of peat compost brill (75%):clay (15%):perlite (10%), under a thermoperiod of 25°C/18°C (day/night), with 14 h light at 4000–6000 Lx and 50%–70% relative humidity, as the optimal climate. Plants were watered daily and fed every week with 12-12-17 N-P-K fertilizer (Compo, Benelux N.V.). Climate switches were applied progressively over a 4-day period. For heat-stress experiments, plants were grown for 5 weeks under optimal temperature. At the onset of flowering, all pre-existing flowers were removed and the thermoperiod was switched to high temperatures. Under 32°C/26°C (day/night), M82/pf1 mutants set no fruits. We then tested 32°C/24°C (day/night), 16/8 h (light/dark) photoperiod, 50%–70% relative humidity. Plants were kept for 4 weeks under these conditions and then 2 weeks under optimal temperatures before harvest. Fruit set was almost completely abolished in the WT M82 line, whereas it was still effective in the parthenocarpic *pf1* mutant. These conditions, 32°C/24°C (day/night), were used for all the heat stress assays. For cold stress, plants were grown under optimal temperatures for 3 weeks and then switched before flowering onset to 15°C/12°C (day/night) temperature, 10/14 h (light/dark) photoperiod, and 60%–70% relative humidity (cold stress conditions), kept for 8 weeks at cold, and then switched back to optimal temperatures for 3 more days before harvest. Winter field tests were carried out from November to April. The plants were grown in soil, under insect-proof plastic tunnels, with natural light and temperature conditions. No measures were taken to enhance pollination. Average temperature did not exceed 15°C for the first 2 months of the trial; hence, it was below the threshold for pollinated fruit set.

Plant crosses and phenotyping

Flowers were emasculated 2 days before anthesis to prevent self-pollination. For F1 crosses, emasculated flowers were manually pollinated 2 days after emasculation using *pf1/pf1* pollen. WT M82, the Simbad elite, and a cherry elite tomato line were used as female recipients for *pf1/PF1* backcrosses and *pf1-3*, *pf1-6*, *pat*, or *pat-1* homozygotes for the *pf1/pf1-3*, *pf1/pf1-6*, *pf1/pat*, and *pf1/pat-1* compound heterozygotes. F1 hybrids were self-pollinated and the phenotypes of F2 plants were compared with those of F1 hybrids and their respective parent lines.

For each *pf1* allele, parthenocarpy was first assessed for more than 10 emasculated flowers per plant, 10 F2 plants per genotype

(WT, homozygote, heterozygote, or compound heterozygote), cultivated in an insect-proof environment. The percentage of developed fruits and seed content were determined at the red-fruit stage. As the WT M82 tomato line develops no seedless fruits, parthenocarpy in *Pf1* M82 can also be scored without emasculation, by counting the seedless fruits produced from plants, vibrated or not. Phenotyping under heat and cold stress conditions was performed on at least eight plants per genotype and condition. Buzz pollination was applied every day for 6 weeks from the onset of blooming, while no measures were taken to enhance pollination in the "non-vibrated" lots.

Tomato productivity was assessed by harvesting and counting the number of red ripe and green fruits per plant. The percentage of seedless fruits was assessed on the total amount of ripe fruits for the greenhouse assays. For the field assays, all of the fruits were harvested and weighed to estimate the yields. Individual fruit weight and presence of seeds were evaluated on ~50 fruits per plot. Total soluble solid contents (Brix index) were assessed with a digital refractometer, in juice squeezed from 8 to 12 individual fruits per plant, collected from six to eight parthenocarpic and six to eight non-parthenocarpic sib plants and four different sibling replicates.

The ovule phenotype was characterized by light microscopy or scanning electron microscopy, on anthesis flowers in three replicate experiments. The correlation of aberrant ovules and parthenocarpy was asserted at the inflorescence level, by dissecting and phenotyping the ovary of one or two anthesis flowers and letting the rest of the same inflorescence develop into parthenocarpic fruits as internal controls.

DNA and RNA preparation

Genomic DNA was extracted from leaf using the DNeasy Plant kit (Qiagen) and total RNA with the Mirvana Kit (Ambion). RNA was purified from leaf, total flower at stages 1–6 (≤1 mm), 8 (2 mm), 9 (3 mm), 11 (4 mm), 12 (5 mm), 13 (6 mm), 15 (7 mm), and 16 (8 mm). RNA was also purified from stage 20 dissected ovaries, ovules, ovules plus placenta, or pericarp and from pollinated flowers at different days after pollination. Shoot–apex RNA was prepared from M82 or *pf1-6*/*pf1-6* seedlings and cultivated for 18 days under optimal temperature followed by 3 days under cold stress for the 15°C samples. The growth being markedly slowed down in cold, the 25°C control apices were collected after 1 more day under optimal conditions (hence 19-day-old seedlings) instead of 3 days. Three shoot apices exhibiting several meristematic bulges under the stereoscope, and hence at the floral transition stage, were bulked for each sample. Ovules alone or ovules plus placenta were dissected under the stereoscope, using razor blades, and frozen in liquid nitrogen. Ovule RNAs were prepared from ovules isolated from 10 WT or 15 *pf1* dissected ovaries. The flower developmental stages were assessed according to Brukhin et al. (2003).

Bulk genomic DNA sequencing and analysis

Equal amounts of genomic DNA from 10 mutant (P) and 10 non-parthenocarpic (NP) F2 segregants were separately bulked. Genomic DNA libraries were constructed following the standard Illumina protocol. The libraries were sequenced on a HiSeq2000. Sequences were trimmed using a Trimmomatic (Bolger et al., 2014) and mapped to the Heinz genome (Tomato Genome Consortium, 2012) (SL3.0) using CLC-Bio (Qiagen), with the following parameters: no_masking, match_score = 1, mismatch_cost = 2, insertion_cost = 3, deletion_cost = 3, length_fraction = 1, similarity_fraction = 0.987. Variants were called initially by retaining high-quality biallelic SNPs with a >0.1 index, in regions covered by at least five reads. Called SNPs were then filtered for EMS-type variants, monomorphic in bulk P as expected for a recessive mutation. A Δ(SNP-index), subtracting bulk-NP!!! SNP index from bulk-P!!! SNP index (Fekih et al., 2013), was computed, enabling us to filter out most variants corresponding to Heinz alleles, or sequencing or mapping errors, revealing the causal mutation.

Phylogenetic analysis

Protein sequences closely homologous to PF1 were isolated from the tomato and *Arabidopsis* genomes, using the Sol Genomics Network (ITAG3.0 release, http://solgenomics.net/) and The Arabidopsis Information Resource (http://www.arabidopsis.org), by BLAST using a set E value of $<1 \times 10^{-10}$. All *Arabidopsis* and tomato HD-ZipIII proteins were aligned under ClustalW (http://www.ebi.ac.uk/Tools/clustalw). Phylogenetic trees were constructed in MEGA7 (Kumar et al., 2016) (http://www.megasoftware.net/index.html), using the maximum likelihood method based on the JTT matrix-based model (Jones et al., 1992). The statistical significance of clades was evaluated with 1000 bootstrap replicates using the same search criteria.

TILLING screening

PF1 TILLING alleles were isolated from an EMS-mutant population of *S. lycopersicum* cv. M82 described previously (Piron et al., 2010) and from a newly generated collection totaling 10 000 M2 families. Both populations were screened by the ENDO1-endonuclease mismatch-detection system as described previously (Piron et al., 2010) or by direct sequencing of target amplicons on a MiSeq system (Illumina) with the primers listed in Supplemental Table 5. The putative impact of the TILLING missense alleles on protein function was predicted using the SIFT program (Sim et al., 2012). Induced mutations predicted to have an impact on the function of the protein were backcrossed to the WT, and the segregation of the mutations with the phenotype was analyzed in F2 plants.

CRISPR-Cas9 gene editing

A guide RNA (gRNA) targeting the *PF1* fifth exon was designed using CRISPR-P (Lei et al., 2014) and joined with the scaffold gRNA and U26 promoter by PCR. Two PCR fragments based on (scafRNA_F, scafRNA_R) and (U26_F, U26_R) primers were amplified from the pCHIMERA plasmid (Leibman-Markus et al., 2018) and combined in a third PCR with (U26_F, scafRNA_R). The resulting product was *Avr*II digested and cloned into the *Avr*II and *Stu*I sites of the pMR286 binary vector (Leibman-Markus et al., 2018). *Agrobacterium tumefaciens* strain *LBA4400*, *VirG*, harboring the pMR286/*PF1* sgRNA recombinant vector was used for *S. lycopersicum* cv. M82 transformation as described (Fernandez et al., 2009). Oligonucleotide sequences are listed in Supplemental Table 5.

Quantitative RT-PCR

First-strand cDNA synthesis was performed according to the manufacturer's protocol with Superscript II (Invitrogen) at 43°C in a 20-μl reaction containing 400 ng total RNA and dT20VN primer, except for the seedling–apex RNA reverse transcribed with Superscript IV (Invitrogen) at 51°C in 20 μl with 70 ng total RNA, 2.5 μM dT20VN, 0.2 μM miR166a_Rt, and 0.2 μM miR166c_Rt. qPCR was performed with 15-fold diluted cDNA using the MESA-green qPCR mix (Eurogentec) and 0.3 μM gene-specific primers, on a CFX384 system (Bio-Rad). The expression of HD-ZipIIIs was analyzed by droplet digital PCR, using the Evagreen Supermix and a QX200 PCR system (Bio-Rad). Actin (Solyc03g078400) was used as a reference gene. Oligonucleotide sequences are listed in Supplemental Table 5. The qPCR results were analyzed using a ΔΔCt methodology. The flower developmental stages were assessed according to Brukhin et al. (2003).

In situ hybridization and histology

In situ hybridizations were performed as described (Nikovics et al., 2006), using a *PF1*-specific riboprobe, a *miR166*-specific LNA probe, or a mouse miR LNA probe as negative control. Oligonucleotides are listed in Supplemental Table 5. Histology analyses on ovaries, of plants harboring different *PF1* alleles, were carried out on a Zeiss LSM880, as described previously (Fonouni-Farde et al., 2019). The flower developmental stages were assessed according to Brukhin et al. (2003).

Auxin measurement

Dissected ovaries in three biological replicates were used for measurement of auxin content. For each sample, 5 mg of dry powder was used. One nanogram per sample of indole-3-acetic acid stable labeled isotopes was used as internal standards as described in Le Roux et al. (2014). Auxin extractions and measurements were carried out as described in Ligerot et al. (2017).

Ethylene measurement

Dissected ovaries in three biological replicates were used for measurement of ethylene production. Ovaries at each stage were dissected, weighed, and enclosed in a 10-ml glass chromatography vial incubated in darkness at 25°C for 2 h. The vials were flushed with hydrocarbon-free air (Air Liquide) at a flow rate of 3 l h^{-1} and ethylene in the headspace was measured with an ETD-300 photoacoustic detector (Sensor Sense B.V., Nijmegen, Netherlands).

DAP-seq analysis

For DAP-seq, the *PF1* CDS was isolated from flower RNA by RT-PCR with (Tom277, Tom278) and joined to Gateway cloning sites by PCR with (Tom029, Tom030) primers. The resulting product was cloned into pDONOR222 and transferred into pIX-HALO by Gateway recombination according to the manufacturer's protocol (Invitrogen). Expression of Halo-PF1 fusion and enrichment of DNA targets were performed as described previously (O'Malley et al., 2016). DNA library preparations were performed following the manufacturer's protocol (Illumina) and sequenced on a NextSeq500 as 2 × 75 nt reads.

Electrophoretic mobility-shift assay

The full-length coding sequence of SlHB15A was cloned into the GST fusion vector pDEST15 and introduced into *E. coli* strain BL21 Rosetta. The GST::SlHB15A recombinant protein or GST tag alone were induced in a 500-ml expression culture using 0.4 mM isopropyl β-D-1-thiogalactopyranoside, and cells were harvested 16 h after induction at 18°C. Cells were lysed using a combination of lysozyme treatment and sonication. Supernatant of the centrifuged lysate was used for GST-tag affinity purification using 0.5 ml Protino Glutathione Agarose 4B medium (Macherey-Nagel). Eluates were analyzed by SDS–PAGE and Coomassie brilliant blue staining. Protein concentration was determined by the Bradford assay (Bradford, 1976). Probes harboring *cis* elements were synthesized and labeled with biotin at their 5′ end. For probe competition, unlabeled probe was added to the reactions. EMSA was performed using the LightShift chemiluminescent EMSA kit (Thermo Fisher Scientific, USA) with 7 μg of recombinant protein per binding reaction. Probe sequences are listed in Supplemental Table 5.

RNA-sequencing analysis

Flower and ovule RNA sequencing (RNA-seq) libraries were constructed according to Illumina instructions and sequenced on HiSeq 4000 platform at Novogene Co. Ltd. Raw sequencing reads were cleaned by removing adaptor sequences and low-quality reads. The resulting high-quality reads were mapped to the tomato genome (Tomato Genome Consortium, 2012) (ITAG3.2) using STAR, with default parameters. Gene expression was quantified using featureCounts with default parameters (Liao et al., 2014). Read count normalization and differential expression analysis were performed using DESeq2 (Love et al., 2014). DEGs in *pf1* ovules compared with WT, with adjusted $P \leq 0.01$ and ratio ≥ 2 or ratio ≤ 0.5, were filtered for subsequent analyses.

For the fertilized and unfertilized WT M82 ovules collected at 1, 2, or 5 DAA, RNA-seq data were retrieved from the NCBI's Gene Expression Omnibus, accession no. GSE72216 (Zhang et al., 2016). Bioinformatic analysis of GSE72216 data was done as described above.

Gene list comparison and Venn diagrams were performed online at http://bioinformatics.psb.ugent.be/webtools/Venn. The statistical significance of the overlaps was calculated using the hypergeometric test (http://nemates.org/MA/progs/overlap_stats.html). Analysis of GO term enrichment was performed using ShyniGO (Ge et al., 2020).

Statistical analyses

All experiments were carried out in at least three replicates. The fruit-set phenotype was analyzed in randomized block design experiments. Student's *t*-test, Tukey's test, and hypergeometric test were used to assess the statistical significance of the results, as described in the above corresponding sections of the methods, the supplemental methods, and the figure legends.

ACCESSION NUMBERS

Raw sequence data from this study have been deposited in the NCBI Short Read Archive database under the following accession numbers: SAMN16792678, SAMN16792679 (bulked-genome sequence from *pf1* parthenocarpic and non-parthenocarpic plants); SAMN16792680 to SAMN16792685 (DAP-seq); SAMN16792686, SAMN16792687, SAMN16816096 to SAMN16816099, and SAMN18442419 to SAMN18442423 (RNA-seq). All *de novo pf1* mutant alleles from this study are available with standard MTA upon request.

SUPPLEMENTAL INFORMATION

Supplemental information is available at *Molecular Plant Online*.

FUNDING

The work was supported by INRAE, CNRS, and the LabEx Saclay Plant Sciences–SPS (ANR-10-LABX-40-SPS). The A.B. team received funding from the European Research Council (ERC-SEXYPARTH, 341076) and from the Horizon 2020 research and innovation program (TOMRES, 727929).

AUTHOR CONTRIBUTIONS

C.C. conceived, conducted, and analyzed the experiments and interpreted the results. C.C., JC.L., S.K., and Y.H. contributed to genetic and phenotypic characterization of the mutants. C.C., A. Boualem, and A. Bendahmane contributed to bulk-genome sequence analysis. F.M. and C.C. contributed to the TILLING screen. H.M., C.C., and Y.H. contributed to histology, scanning electron microscopy, and *in situ* hybridizations, which were analyzed by C.C.; C.C. and Y.H. performed qPCR expression studies; A. Boualem, C.C., B.M., and M.V. contributed to RNA-seq. R.B. and R.S.D. performed CRISPR and DAP-seq experiments. A. Boualem, M.V., and C.C. analyzed the DAP-seq data. C.C. and R.S.D. contributed to the EMSA. C.C., S.C., and G.M. contributed to the auxin analysis. C.C. and G.B. contributed to the ethylene analysis. A. Bendahmane conceived and supervised the study. C.C. and A. Boualem prepared the figures. C.C. and A. Bendahmane wrote the manuscript with contribution from A. Boualem. All authors read and approved the final manuscript.

ACKNOWLEDGMENTS

We thank Martin Crespi and Reiner Veitia for fruitful discussions; Judit Szecsi and Youssef Belkhadir for careful proofreading of the manuscript; and Afef Lemhamdi, Julien Brunel, Pascal Audigier, and Holger Ornstrup for technical assistance. The authors have no conflicts to declare.

Received: November 9, 2020
Revised: March 22, 2021
Accepted: May 3, 2021
Published: May 4, 2021

REFERENCES

Abdul-Baki, A.A., and Stommel, J.R. (1995). Pollen viability and fruit set of tomato genotypes under optimum and high-temperature regimes. HortScience **30**:115.

Bolger, A.M., Lohse, M., and Usadel, B. (2014). Trimmomatic: a flexible trimmer for Illumina sequence data. Bioinformatics **30**:2114–2120.

Bradford, M.M. (1976). A rapid and sensitive method for the quantita- tion of microgram quantities of protein utilizing the principle of protein- dye binding. Anal. Biochem. **72**:248–254.

Brandt, R., Salla-Martret, M., Bou-Torrent, J., Musielak, T., Stahl, M., Lanz, C., Ott, F., Schmid, M., Greb, T., Schwarz, M., et al. (2012). Genome-wide binding-site analysis of REVOLUTA reveals a link between leaf patterning and light-mediated growth responses. Plant J. **72**:31–42.

Brukhin, V., Hernould, M., Gonzalez, N., Chevalier, C., and Mouras, A. (2003). Flower development schedule in tomato Lycopersicon esculentum cv. sweet cherry. Sex. Plant Reprod. **15**:311–320.

Carbonell-Bejerano, P., Urbez, C., Granell, A., Carbonell, J., and Perez-Amador, M.A. (2011). Ethylene is involved in pistil fate by modulating the onset of ovule senescence and the GA-mediated fruit set in Arabidopsis. BMC Plant Biol. **11**:84.

Charles, W.B., and Harris, R.E. (1972). Tomato fruit-set at high and low temperatures. Can. J. Plant Sci. **52**:497–506.

Cooper, D.C. (1931). Macrosporogenesis and the development of the macrogametophyte of lycopersicon Esculentum. Am. J. Bot. **18**:739–748.

da Silva, E.M., Silva, G.F.F.E., Brussolo Bidoia, D., da Silva Azevedo, M., Almeida de Jesus, F., Pino, L.E., Peres, L.E.P., Carrera, E., Lopez-Diaz, I., and Nogueira, F.T.S. (2017). microRNA159-targeted SlGAMYB transcription factors are required for fruit set in tomato. Plant J. **92**:95–109.

de Jong, M., Wolters-Arts, M., Feron, R., Mariani, C., and Vriezen, W.H. (2009). The Solanum lycopersicum auxin response factor 7 (SlARF7) regulates auxin signaling during tomato fruit set and development. Plant J. **57**:160–170.

Deutschbauer, A.M., Jaramillo, D.F., Proctor, M., Kumm, J., Hillenmeyer, M.E., Davis, R.W., Nislow, C., and Giaever, G. (2005). Mechanisms of haploinsufficiency revealed by genome-wide profiling in yeast. Genetics **169**:1915–1925.

Dorcey, E., Urbez, C., Blázquez, M.A., Carbonell, J., and Perez-Amador, M.A. (2009). Fertilization-dependent auxin response in ovules triggers fruit development through the modulation of gibberellin metabolism in Arabidopsis. Plant J. **58**:318–332.

Erickson, A.N., and Markhart, A.H. (2002). Flower developmental stage and organ sensitivity of bell pepper (Capsicum annuum L.) to elevated temperature. Plant Cell Environ. **25**:123–130.

Fekih, R., Takagi, H., Tamiru, M., Abe, A., Natsume, S., Yaegashi, H., Sharma, S., Sharma, S., Kanzaki, H., Matsumura, H., et al. (2013). MutMap+: genetic mapping and mutant identification without crossing in rice. PLoS One **8**:e68529.

Fernandez, A.I., Viron, N., Alhagdow, M., Karimi, M., Jones, M., Amsellem, Z., Sicard, A., Czerednik, A., Angenent, G., Grierson, D., et al. (2009). Flexible tools for gene expression and silencing in tomato. Plant Physiol. **151**:1729–1740.

Firon, N., Shaked, R., Peet, M.M., Pharr, D.M., Zamski, E., Rosenfeld, K., Althan, L., and Pressman, E. (2006). Pollen grains of heat tolerant tomato cultivars retain higher carbohydrate concentration under heat stress conditions. Sci. Hortic. **109**:212–217.

Fonouni-Farde, C., Miassod, A., Laffont, C., Morin, H., Bendahmane, A., Diet, A., and Frugier, F. (2019). Gibberellins negatively regulate the development of Medicago truncatula root system. Sci. Rep. **9**:2335.

Garcia-Hurtado, N., Carrera, E., Ruiz-Rivero, O., López-Gresa, M.P., Hedden, P., Gong, F., and García-Martínez, J.L. (2012). The characterization of transgenic tomato overexpressing gibberellin 20-oxidase reveals induction of parthenocarpic fruit growth, higher yield, and alteration of the gibberellin biosynthetic pathway. J. Exp. Bot. **63**:5803–5813.

Ge, S.X., Jung, D., and Yao, R. (2020). ShinyGO: a graphical gene-set enrichment tool for animals and plants. Bioinformatics **36**:2628–2629.

Giorno, F., Wolters-Arts, M., Mariani, C., and Rieu, I. (2013). Ensuring reproduction at high temperatures: the heat stress response during anther and pollen development. Plants (Basel) **2**:489–506.

Gomez, M.D., Ventimilla, D., Sacristan, R., and Perez-Amador, M.A. (2016). Gibberellins regulate ovule integument development by interfering with the transcription factor ATS. Plant Physiol. **172**:2403–2415.

Gomez, M.D., Barro-Trastoy, D., Escoms, E., Saura-Sánchez, M., Sánchez, I., Briones-Moreno, A., Vera-Sirera, F., Carrera, E., Ripoll, J.-J., Yanofsky, M.F., et al. (2018). Gibberellins negatively modulate ovule number in plants. Development **145**:163865.

Hao, S., Ariizumi, T., and Ezura, H. (2017). SEXUAL STERILITY is essential for both male and female gametogenesis in tomato. Plant Cell Physiol. **58**:22–34.

Hashimoto, K., Miyashima, S., Sato-Nara, K., Yamada, T., and Nakajima, K. (2018). Functionally diversified members of the MIR165/6 gene family regulate ovule morphogenesis in Arabidopsis thaliana. Plant Cell Physiol. **59**:1017–1026.

Hu, J., Israeli, A., Ori, N., and Sun, T.P. (2018). The interaction between DELLA and ARF/IAA mediates crosstalk between gibberellin and auxin signaling to control fruit initiation in tomato. Plant Cell **30**:1710–1728.

Johnson, A.F., Nguyen, H.T., and Veitia, R.A. (2019). Causes and effects of haploinsufficiency. Biol. Rev. Camb. Philos. Soc. **94**:1774–1785.

Joldersma, D., and Liu, Z. (2018). The making of virgin fruit: the molecular and genetic basis of parthenocarpy. J. Exp. Bot. **69**:955–962.

Jones, D.T., Taylor, W.R., and Thornton, J.M. (1992). The rapid generation of mutation data matrices from protein sequences. Comput. Appl. Biosci. **8**:275–282.

Jones-Rhoades, M.W., Bartel, D.P., and Bartel, B. (2006). MicroRNAs and their regulatory roles in plants. Ann. Rev. Plant Biol. **57**:19–53.

Kelley, D.R., Skinner, D.J., and Gasser, C.S. (2009). Roles of polarity determinants in ovule development. Plant J. **57**:1054–1064.

Kim, J., Jung, J.H., Reyes, J.L., Kim, Y.S., Kim, S.Y., Chung, K.S., Kim, J.A., Lee, M., Lee, Y., Narry Kim, V., et al. (2005). microRNA-directed cleavage of ATHB15 mRNA regulates vascular development in Arabidopsis inflorescence stems. Plant J. **42**:84–94.

Kumar, S., Stecher, G., and Tamura, K. (2016). MEGA7: molecular evolutionary genetics analysis version 7.0 for bigger datasets. Mol. Biol. Evol. **33**:1870–1874.

Le Roux, C., Del Prete, S., Boutet-Mercey, S., Perreau, F., Balagué, C., Roby, D., Fagard, M., and Gaudin, V. (2014). The hnRNP-Q protein LIF2 participates in the plant immune response. PLoS One **9**:e99343.

Lei, Y., Lu, L., Liu, H.Y., Li, S., Xing, F., and Chen, L.L. (2014). CRISPR-P: a web tool for synthetic single-guide RNA design of CRISPR-system in plants. Mol. Plant **7**:1494–1496.

Leibman-Markus, M., Pizarro, L., Schuster, S., Lin, Z.J.D., Gershony, O., Bar, M., Coaker, G., and Avni, A. (2018). The intracellular nucleotide-binding leucine-rich repeat receptor (SlNRC4a) enhances immune signaling elicited by extracellular perception. Plant Cell Environ. **41**:2313–2327.

Liao, Y., Smyth, G.K., and Shi, W. (2014). featureCounts: an efficient general purpose program for assigning sequence reads to genomic features. Bioinformatics **30**:923–930.

Liu, N., Wu, S., Van Houten, J., Wang, Y., Ding, B., Fei, Z., Clarke, T.H., Reed, J.W., and Esther van der Knaap, E. (2014). Down-regulation of AUXIN RESPONSE FACTORS 6 and 8 by microRNA 167 leads to floral

development defects and female sterility in tomato. J. Exp. Bot. **65**:2507–2520.

Ligerot, Y., de Saint Germain, A., Waldie, T., Troadec, C., Citerne, S., Kadakia, N., Pillot, J.P., Prigge, M., Aubert, G., Bendahmane, A., et al. (2017). The pea branching RMS2 gene encodes the PsAFB4/5 auxin receptor and is involved in an auxin-strigolactone regulation loop. PLoS Genet. **8**:e1007089.

Lopez-Gomollon, S., Mohorianu, I., Szittya, G., Moulton, V., and Dalmay, T. (2012). Diverse correlation patterns between microRNAs and their targets during tomato fruit development indicates different modes of microRNA actions. Planta **236**:1875–1887.

Love, M.I., Huber, W., and Anders, S. (2014). Moderated estimation of fold change and dispersion for RNA-seq data with DESeq2. Genome Biol. **15**:550.

Marti, C., Orzáez, D., Ellul, P., Moreno, V., Carbonell, J., and Granell, A. (2007). Silencing of DELLA induces facultative parthenocarpy in tomato fruits. Plant J. **52**:865–876.

Nikovics, K., Blein, T., Peaucelle, A., Ishida, T., Morin, H., Aida, M., and Laufs, P. (2006). The balance between the MIR164A and CUC2 genes controls leaf margin serration in Arabidopsis. Plant Cell **18**:2929–2945.

Okabe, Y., Yamaoka, T., Ariizumi, T., Ushijima, K., Kojima, M., Takebayashi, Y., Sakakibara, H., Kusano, M., Shinozaki, Y., Imriani Pulungan, S., et al. (2019). Aberrant stamen development is associated with parthenocarpic fruit set through up-regulation of gibberellin biosynthesis in tomato. Plant Cell Physiol. **60**:38–51.

O'Malley, R.C., Huang, S.C., Song, L., Lewsey, M.G., Bartlett, A., Nery, J.R., Galli, M., Gallavotti, A., and Ecker, J.R. (2016). Cistrome and epicistrome features shape the regulatory DNA landscape. Cell **166**:1598.

Omidvar, V., Mohorianu, I., Dalmay, T., and Fellner, M. (2015). MicroRNA regulation of abiotic stress response in 7B-1 male-sterile tomato mutant. Plant Genome **8**, eplantgenome2015.02.0008.

Pattison, R.J., Csukasi, F., Zheng, Y., Fei, Z., van der Knaap, E., and Catalá, C. (2015). Comprehensive tissue-specific transcriptome analysis reveals distinct regulatory programs during early tomato fruit development. Plant Physiol. **168**:1684–1701.

Pecaut, J., and Philouze, J. (1978). A *sha/pat* line obtained by natural mutation. Rep. Tom. Genet. Coop. **28**:12.

Peet, M.M., Sato, S., and Gardner, R.G. (1998). Comparing heat stress effects on male-fertile and male-sterile tomatoes. Plant Cell Environ. **21**:225–231.

Pillitteri, L.J., Bemis, S.M., Shpak, E.D., and Torii, K.U. (2007). Haploinsufficiency after successive loss of signaling reveals a role for ERECTA-family genes in Arabidopsis ovule development. Development **134**:3099–3109.

Piron, F., Nicolai, M., Minoia, S., Piednoir, E., Moretti, A., Salgues, A., Zamir, D., Caranta, C., and Bendahmane, A. (2010). An induced mutation in tomato eIF4E leads to immunity to two potyviruses. PLoS One **5**:e11313.

Rodriguez, G.R., Munos, S., Anderson, C., Sim, S.C., Michel, A., Causse, M., Gardener, B.B., Francis, D., and van der Knaap, E. (2011). Distribution of SUN, OVATE, LC, and FAS in the tomato germplasm and the relationship to fruit shape diversity. Plant Physiol. **156**:275–285.

Rotino, G.L., Perri, E., Zottini, M., Sommer, H., and Spena, A. (1997). Genetic engineering of parthenocarpic plants. Nat. Biotechnol. **15**:1398–1401.

Sato, S., Peet, M.M., and Thomas, J.F. (2000). Physiological factors limit fruit set of tomato (Lycopersicon esculentum Mill.) under chronic, mild heat stress. Plant Cell Environ. **23**:719–726.

Serrani, J.C., Sanjuan, R., Ruiz-Rivero, O., Fos, M., and Garcia-Martinez, J.L. (2007). Gibberellin regulation of fruit set and growth in tomato. Plant Physiol. **145**:246–257.

Serrani, J.C., Ruiz-Rivero, O., Fos, M., and Garcia-Martinez, J.L. (2008). Auxin-induced fruit-set in tomato is mediated in part by gibberellins. Plant J. **56**:922–934.

Shinozaki, Y., Ezura, H., and Ariizumi, T. (2018). The role of ethylene in the regulation of ovary senescence and fruit set in tomato (Solanum lycopersicum). Plant Signal. Behav. **13**:e1146844.

Shinozaki, Y., Beauvoit, P.B., Takahara, M., Hao, S., Ezura, K., Andrieu, M.-H., Nishida, K., Mori, K., Suzuki, Y., Kuhara, S., et al. (2020). Fruit setting rewires central metabolism via gibberellin cascades. Proc. Natl. Acad. Sci. U S A **117**:23970–23981.

Sim, N.L., Kumar, P., Hu, J., Henikoff, S., Schneider, G., and Ng, P.C. (2012). SIFT web server: predicting effects of amino acid substitutions on proteins. Nucleic Acids Res. **40**:W452–W457.

Skinner, D.J., Brown, R.H., Kuzoff, R.K., and Gasser, C.S. (2016). Conservation of the role of INNER NO OUTER in development of unitegmic ovules of the Solanaceae despite a divergence in protein function. BMC Plant Biol. **16**:143.

Soressi, G.P., and Salamini, F. (1975). A monomendellian gene inducing parthenocarpic fruits. Rep. Tom. Genet. Coop. **25**:22.

Tomato Genome Consortium. (2012). The tomato genome sequence provides insights into fleshy fruit evolution. Nature **485**:635–641.

Wang, H., Liu, Y., Bruffett, K., Lee, J., Hause, G., Walker, J.C., and Zhang, S. (2008). Haplo-insufficiency of MPK3 in MPK6 mutant background uncovers a novel function of these two MAPKs in Arabidopsis ovule development. Plant Cell **20**:602–613.

Wang, H., Schauer, N., Usadel, B., Frasse, P., Zouine, M., Hernould, M., Latche, A., Pech, J.C., Fernie, A.R., and Bouzayen, M. (2009). Regulatory features underlying pollination-dependent and -independent tomato fruit set revealed by transcript and primary metabolite profiling. Plant Cell **21**:1428–1452.

Xu, Q., Li, R., Weng, L., Sun, Y., Meng, L., and Han, X. (2019). Domain-specific expression of meristematic genes is defined by the LITTLE ZIPPER protein DTM in tomato. Commun Biol. **2**:134.

Xu, S., and Chong, K. (2018). Remembering winter through vernalisation. Nat. Plants **4**:997–1009.

Zhang, S., Xu, M., Qiu, Z., Wang, K., Du, Y., Gu, L., and Cui, X. (2016). Spatiotemporal transcriptome provides insights into early fruit development of tomato (Solanum lycopersicum). Sci. Rep. **6**:23173.

Zhang, T., Li, Y., Ma, L., Sang, X., Ling, Y., Wang, Y., Yu, P., Zhuang, H., Huang, J., Wang, N., et al. (2017). LATERAL FLORET 1 induced the three-florets spikelet in rice. Proc. Natl. Acad. Sci. U S A **114**:9984–9989.

Zhao, C., Liu, B., Piao, S., Wang, X., Lobell, D.B., Huang, Y., Huang, M., Yao, Y., Bassu, S., Ciais, P., et al. (2017a). Temperature increase reduces global yields of major crops in four independent estimates. Proc. Natl. Acad. Sci. U S A **114**:9326–9331.

Zhao, X., Bramsiepe, J., Van Durme, M., Komaki, S., Prusicki, M.A., Maruyama, D., Forner, J., Medzihradszky, A., Wijnker, E., Harashima, H., et al. (2017b). RETINOBLASTOMA RELATED1 mediates germline entry in Arabidopsis. Science **356**:eaaf6532.

Zinn, K.E., Tunc-Ozdemir, M., and Harper, J.F. (2010). Temperature stress and plant sexual reproduction: uncovering the weakest links. J. Exp. Bot. **61**:1959–1968.